Reductive Activation of the Nitrogen Molecule at the Surface of "Electron-Rich" MgO and CaO. The N_2^- Surface Adsorbed Radical Ion

Mario Chiesa,[†] Elio Giamello,*[,‡] Damien M. Murphy,[†] Gianfranco Pacchioni,[§] M. Cristina Paganini,[‡] Raffaella Soave,[§] and Zbigniew Sojka[||]

Dipartimento di Chimica IFM, Università di Torino, e Unità INFM di Torino, Via Giuria, 7-10125 Torino, Italia, Dipartimento di Scienza dei Materiali, Universita' degli Studi di Milano-Bicocca, e Unità INFM di Milano, via Cozzi, 53-20125 Milano, Italy, Department of Chemistry, Cardiff University, P.O. Box 912, Cardiff CF10 3TB, U.K., and Department of Chemistry, Jagiellonian University, ul. Ingardena, 3, Cracow, Poland

Received: August 2, 2000; In Final Form: November 2, 2000

Upon nitrogen adsorption at low temperature onto the surface of magnesium oxide and calcium oxide containing F_S^+ centers (single electron trapped in a suitable surface vacancy), electron transfer occurs from the solid to the adsorbed molecule. About 90% of the total electron density is localized on the adsorbed molecule. The 11-electron N_2^- radical anion so formed has been detected by electron paramagnetic resonance for both $^{14}N_2$ and $^{15}N_2$. The electron transfer is reversible and, when the pressure is lowered or the temperature increased, the N_2 molecules desorb, regenerating the original F_S^+ center. The diatomic radical ion lies parallel to the surface, and the electron density is mainly confined in the π_y^* orbital. Theoretical calculations at the DFT level indicate that a small energy barrier separates the unbound F_S^+/N_2 state from the bound F_S^{2+}/N_2^- state. This explains the facile reversibility of the electron-transfer process. The calculated spin densities are in excellent agreement with those derived from the experiments. The results reported in this paper represent a new method for N_2 activation over the basic alkaline earth oxides, which are also known to activate H_2 by dissociative adsorption.

1. Introduction

Over the years, the subject of nitrogen fixation has presented a challenging and difficult task for both chemists and biochemists alike. The many and varied approaches adopted for N_2 activation and its resulting transformation into ammonia have delved into various branches of chemistry, including heterogeneous catalysis. Despite the extensive efforts in these various fields, the promoted iron catalyst of the Haber Bosch process remains the only large-scale artificial process for ammonia production[1]. Nevertheless, various other routes for dinitrogen activation have developed more recently.[2] These include the following: (1) the use of transition-metal complexes containing terminal or bridging N_2 ligands[3,4] for the preparation of adducts with considerably long N−N bonds which may, in principle, undergo protonation; (2) in the field of biological nitrogen fixation, the characterization (and possibly mimicking) of the structure and catalytic activity of nitrogenase, a multiprotein containing an iron−molybdenum−sulfur cluster, which catalyses the reaction of nitrogen with water in reducing conditions;[5−7] and (3) the development of processes for nitrogen fixation in solution, mainly pioneered by the Russian group of Shilov,[8] using different reaction systems, including mixed V(II)-Mg hydroxides, V(II) complexes with polyphenols, and even sodium amalgam, thereby obtaining either stoichiometric or catalytic conversion of dinitrogen.

The key step in all the above processes is activation of the nitrogen molecule, regardless of the system adopted for achieving this. However, it is critical that the structure and bonding of the activated molecule resulting from these reactions is thoroughly understood. The work illustrated in the present article is therefore loosely related to this important field of dinitrogen activation on heterogeneous systems by providing a comprehensive experimental and theoretical description of the nature of a surface-activated N_2 molecule. The significance of the present work is based on the novelty of the heterogeneous system involved, which is completely different form the promoted iron catalysts or other heterogeneous systems examined until now.[8] As will be demonstrated, reversible reduction of the nitrogen molecule forming an N_2^- radical anion occurs at very low temperatures via a direct electron transfer from particular surface sites on CaO or MgO containing trapped electrons.

The surface chemistry of the basic oxides (MgO and CaO) has been extensively studied in our laboratories both experimentally and theoretically. The physics and chemistry of the surface sites which can trap and stabilize excess electrons was explored after formation by the addition of low ionization energy metals [9,10] or irradiation under chemisorbed hydrogen.[11−14] These "electron-rich" surfaces contain defects known as F_S centers or color centers and, similar to the bulk analogues found in ionic oxides or halides, produce a characteristic blue color. The reactivity of these surface color centers was also examined and was demonstrated to act as powerful reducing agents exhibiting a strong propensity for electron transfer to various adsorbed substrates. The pronounced reducing activity is unusual, however, compared to that of other strong reductants

* To whom the correspondence should be addressed. Telephone: ++39-0116707574. Fax: ++39-0116707855, E-mail: Giamello@ch.unito.it.
[†] Cardiff University.
[‡] Università di Torino.
[§] Universita' degli Studi di Milano-Bicocca.
[||] Jagiellonian University.

10.1021/jp002794+ CCC: $20.00
Published on Web 12/19/2000

such as alkali metals or alkali metals hydrides, since the ionic surface assists the stabilization of the various reactive intermediates, as demonstrated for example for the superoxide radical ions[16,17] or the CO^- and $C_2O_2^-$ anions.[18]

The present article describes how these electron-rich MgO and CaO surfaces create a reduced dinitrogen species at low temperatures. A preliminary communication on this reversibly formed N_2^- radical on MgO was recently reported by us.[19] To understand any surface molecular process, particularly in heterogeneous catalysis, one must be able to model the nature and structure of the active site involved. As demonstrated in this work, electron paramagnetic resonance (EPR) spectroscopy can provide the required sensitivity, resolution, and precision, even using a polycrystalline material with small concentrations of radicals, from the correct identification of the species and its SOMO orbital to the geometrical description of its adsorption site. Simultaneously, the system has also been modeled by ab initio quantum chemistry calculations which verify the proposed reaction pathway and the structure of the anion and explore other properties of the new species not directly observed by experiments.

Finally, it should be noted that under the adopted experimental conditions, both CaO and MgO produce and stabilize the N_2^- radical ion. However, the surfaces of these two alkali-earth oxides can also activate the hydrogen molecule by dissociative adsorption.[13,20] These two facts are the reason that the present work, far from being a report on dinitrogen hydrogenation, has been put in the context of the chemistry of nitrogen fixation.

2. Experimental and Computational Methods

2.1. Experimental Section. High-surface-area (HSA) MgO (ex Johnson Matthey) was produced by thermal decomposition of $Mg(OH)_2$ under dynamic vacuum at 523K for 16 h. The HSA MgO was then activated under a vacuum of 10^{-5} Torr at 1073 K for 1 h to obtain a completely dehydrated material. The surface area of the activated oxide was $\sim 170-200$ m^2 g^{-1}. Some experiments (vide infra) were carried out using MgO obtained by chemical vapor deposition (CVD) in a flow system.[20] The samples were kindly supplied by Prof. Erich Knözinger (Institut für Physikalische Chemie Technische Universität Wien). The surface area of the CVD MgO activated at 1073 K was ~ 320 m^2 g^{-1}.[20] High-surface-area CaO was obtained by the slow decomposition of high-purity $CaCO_3$ powder under dynamic vacuum. The oxide was then activated under vacuum at 1173 K for 1 h. The surface area of the resulting oxide is about 70 m^2 g^{-1}.

The F_S^+(H) or F_S^+(D) color centers were generated on the surface of the activated oxides as described in detail elsewhere.[9−14] Hydrogen or deuterium ($\sim$100 Torr, 1 Torr = 133 Pa) was added to the activated oxide at 298 K, and the powder was subsequently cooled to 77 K. The sample was then irradiated using a low-pressure UV mercury vapor lamp for about 1 h. The excess H_2 or D_2 was then slowly evacuated at 298 K from the pale-blue-colored sample before recording the EPR spectrum. High-purity $^{14}N_2$ and $^{15}N_2$ gases (ex Cambridge Isotopes) were used without further purification.

X-band CW-EPR spectra were recorded at 298 and 77 K on a Varian E-109 spectrometer equipped with a cylindrical cavity operating at a 100 kHz field modulation. Varian pitch ($\mathbf{g} = 2.0028$) was used for **g** value calibration. The EPR computer simulations were obtained using a program adapted for a personal computer and derived from the SIM14S program.

2.2. Computational Method. The interaction of N_2 with the surface F_S center on MgO was limited to the simple case of a one-electron F_S^+ center at the planar (100) face. Although the centers investigated by EPR are F_S^+(H) centers (containing a weakly interacting proton from a nearby OH group), this difference does not significantly influence (vide infra) the interaction between the nitrogen molecule and the trapped electron center (F_S^+ or F_S^+(H) centers).

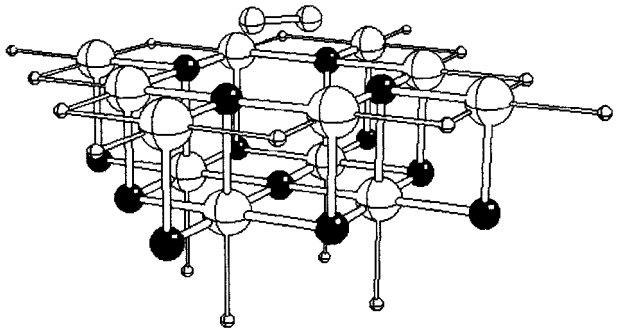

Figure 1. $O_{12}Mg_{13}$ cluster model of an oxygen vacancy on the MgO surface adopted to describe the interaction of N_2 with the F_S^+ center. White spheres, O; black spheres, Mg; small gray spheres, ECPs; large gray spheres, N.

The interaction of N_2 with an F_S^+ center on the (001) MgO surface was already studied using cluster models and first-principle quantum-chemical calculations.[19] This approach has been widely used to study adsorption and reaction of gas-phase molecules with oxide surfaces.[21−23] The truncation of the lattice in cluster models of ionic materials implies the use of external fields to represent the long-range Coulomb potential.[24] In this work, we have represented the Madelung potential of the crystal by means of a large array of point charges (PC). A disadvantage of this technique is that the PCs cause an artificial polarization of the ions at the cluster border, in particular the oxide anions, resulting in an incorrect behavior of the electrostatic potential in the adsorption region.[25] A way of circumventing the problem is to place at the position of the +2 PCs around the cluster an effective core potential (ECP) which provides a simple representation of the finite size of the Mg^{2+} core.[26−28] No basis functions are associated to the ECP,[29] which has the effect of taking into account the Pauli or exchange repulsion of the O^{2-} valence electrons with the surrounding. This is a simplified approach with respect to the more rigorous embedding schemes proposed by Sejio and Barandiaran [30] or to the Greens function method of Pisani.[31] On the other hand, the cluster approach is computationally simple, parameter free, and sufficiently reliable, in particular for ionic surfaces such as MgO. In this work, the F_S^+ center has been modeled by a $[O_{12}Mg_{13}]$ cluster (Figure 1), surrounded by 16 ECPs and 634 ± 2 PCs.

For the calculations, we have adopted two methods: the Hartree−Fock (HF) and the gradient-corrected density functional theory (DFT-GGA). In DFT, we used the hybrid Becke3 functional for exchange[32] and the Lee−Yang−Parr functional for correlation,[33] B3LYP. As shown in a previous paper,[19] HF is sufficient for a qualitative analysis, since electrostatic effects dominate the interaction of F centers with N_2. On the other hand, DFT calculations, where correlation effects are taken into account, are needed for a more quantitative description, in particular of the energetics. Open-shell systems have been described by unrestricted HF (UHF) or spin-polarized DFT. In all cases, the computed spin functions are almost pure doublets ($\langle S^2 \rangle = 0.750 \pm 0.002$). The interaction of N_2 with the F_S^+ center has been studied by computing sections of the potential energy surface and by full gradient optimizations. This latter procedure can provide more quantitative comparisons with experimental data. During the geometry optimizations, the two

SCHEME 1

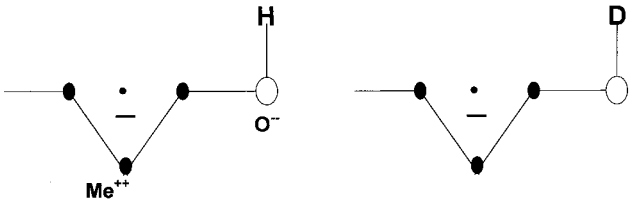

N atoms, all the O^{2-} anions, and four surface Mg^{2+} cations of the cluster are free to move, while the rest is fixed at bulk positions.

Gaussian-type atomic orbital basis sets have been used to construct the HF and the Kohn−Sham orbitals. The choice of the basis set is a delicate problem because of the uncertain description of the N_2 electron affinity (EA), for which there is no experimental estimate. We have calibrated our calculations by using the EA value of −2.00 eV reported by Gutsev et al.[34] with very accurate quantum-mechanical calculations. For the description of N_2, we used the 6-311+G* basis set, which gives an EA of −1.61 eV; with this basis set, the N_2 dissociation energy, 9.75 eV, is almost coincident with the experimental one, 9.80 eV. The O atoms of the cluster have been treated with the 6-31G basis set[35] and the five Mg ions around the vacancy with a 6-31++G basis set, while the remaining Mg ions have been described with a 6-31G basis from which the most diffuse s and p orbitals have been removed. No floating functions have been placed in the center of the vacancy since, as we will discuss in a forthcoming paper, the basis adopted for the Mg ions around the vacancy efficiently describes the localization of the unpaired electron inside the F_S center. All the binding energies of N_2 with the surface have been corrected by the basis set superposition error (BSSE).[36]

The hyperfine coupling constants for the interaction of the electron spin with the nuclear spin of ^{14}N in the complex F_S^{2+}/N_2^- have been determined both at the HF and DFT-B3LYP levels. The calculations have been performed with the HONDO 8.5[37] and the Gaussian98[38] program packages.

3. Results and Discussion

3.1. Species Formed by N_2 Adsorption. Following UV irradiation at 77K under a hydrogen or deuterium atmosphere, the thoroughly dehydrated oxide (MgO and CaO give similar results) changes color from white to pale blue. This blue color is typical of surface-trapped electron centers, including the two-electron neutral F_S(H) centers and the one-electron paramagnetic F_S^+(H) centers. The corresponding F_S(D) and F_S^+(D) centers are formed after irradiation under a deuterium atmosphere. The EPR features of these paramagnetic color centers, the nature of the surface site (shown in Scheme 1), and the associated chemical processes involved in their formation have been described in previous papers.[9−15] The EPR spectrum of the F_S^+-(D) center on CaO is shown in Figure 2a. It consists of a narrow, slightly asymmetric signal due to the axial nature of the **g** tensor component. The hyperfine structure due to the unpaired electron interacting with the D nucleus of the neighboring OD group is not resolved in Figure 2a. Adsorption of N_2 (100 Torr) at low temperature significantly alters the spectrum, and a new signal appears, shown in Figure 2b. At these temperatures, approximately one monolayer of N_2 is physically adsorbed on the surface. The new spectrum in Figure 2b arises from the reversible interaction of the adsorbate with the surface, since the original F_S^+(D) signal is immediately restored (Figure 2c)

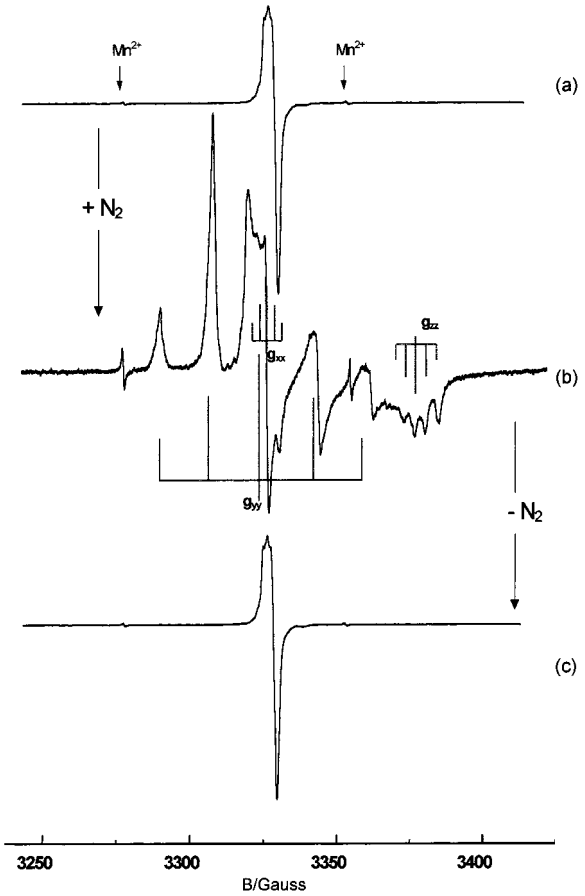

Figure 2. The effect of $^{14}N_2$ adsorption on the surface of CaO containing F_S^+(D) centers. From top to bottom: (a) EPR spectrum of F_S^+(D); (b) EPR spectrum after N_2 addition with stick-diagram of the species with two equivalent N nuclei; (c) EPR spectrum after N_2 desorption. All the spectra have been recorded at 77 K. The small arrows indicate the lines due to Mn^{2+} impurities in CaO.

upon evacuation. A spectrum similar to that shown in Figure 2b was recently reported by us using MgO[19] and assigned to the adsorbed N_2^- radical anion. It is clear, therefore, that the N_2^- anion is also formed on the electron-enriched CaO surface. This assignment on both surfaces will now be corroborated and discussed in significant detail.

3.2. EPR Spectra of the Species Formed by N_2 Adsorption. The spectrum in Figure 2b was simulated using the following spin−Hamiltonian:

$$H = \mu_B \mathbf{BgS} + \mathbf{SAI}_a + \mathbf{SAI}_b \qquad (1)$$

The experimental and simulated spectra of the N_2^- anion are shown in panels a and b of Figure 3, respectively. The spin Hamiltonian parameters employed in the simulation are listed in Table 1. The simulated spectrum was obtained using a single $S = {}^1/_2$ species having rhombic **g** and **A** tensors, with two **g** values close to that of the free spin and one **g** value lower (1.9677). A 10% fraction of original F_S^+(D) center remains unreacted after N_2 adsorption, and its profile was included in the simulation. The observed hyperfine structure is typical of two equivalent ^{14}N nuclei ($I = 1$) producing a quintuplets pattern with the intensity ratio of 1:2:3:2:1 (see stick diagram in Figure 2b). This assignment was confirmed using $^{15}N_2$ ($I = {}^1/_2$), which produced the expected triplet pattern with a 1:2:1 ratio (Figure 3c,d). The simulated spectrum of $^{15}N_2^-$ (Figure 3d) was derived on the basis of the same **g** tensor values used for $^{14}N_2^-$ and after adjusting the coupling constants by the appropriate ratio

TABLE 1: Spin−Hamiltonian Parameters for N_2^- Radical Anions Adsorbed on MgO and CaO and Trapped in the Bulk of Different Azides

	g_{xx}	g_{yy}	g_{zz}	A_{xx} (G)	A_{yy} (G)	A_{zz} (G)	ref.
$^{14}N_2^-$ on MgO	2.0018	2.0042	1.9719	2.90	21.50	4.20	this work
$^{15}N_2^-$ on MgO	2.0018	2.0042	1.9719	4.06	30.10	5.88	this work
$^{14}N_2^-$ on CaO	2.0006	2.0048	1.9677	2.50	20.00	4.30	this work
$^{15}N_2^-$ on CaO	2.0006	2.0048	1.9677	3.50	28.00	6.02	this work
N_2^- in KN_3	2.0008	2.0027	1.9832	3.8	12.0	4.0	40
N_2^- in NaN_3	∼2.00	∼2.00	1.75	11.0	23.5	3.9	41
N_2^- in $Ba(N_3)_2$	∼1.99	∼1.99	1.979	3.6	20.7	4.1	42

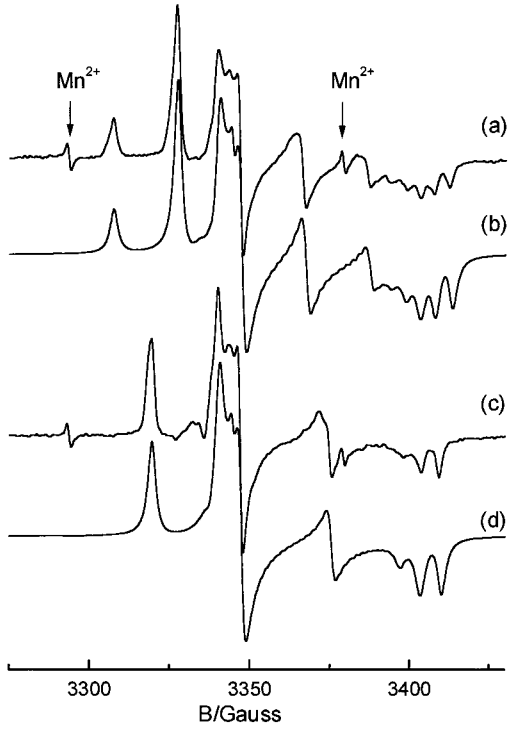

Figure 3. Experimental (a) and simulated (b) EPR spectra of $^{14}N_2^-$ on CaO. Experimental (c) and simulated (d) EPR spectra of $^{15}N_2^-$ on CaO. Spectra recorded at 77 K.

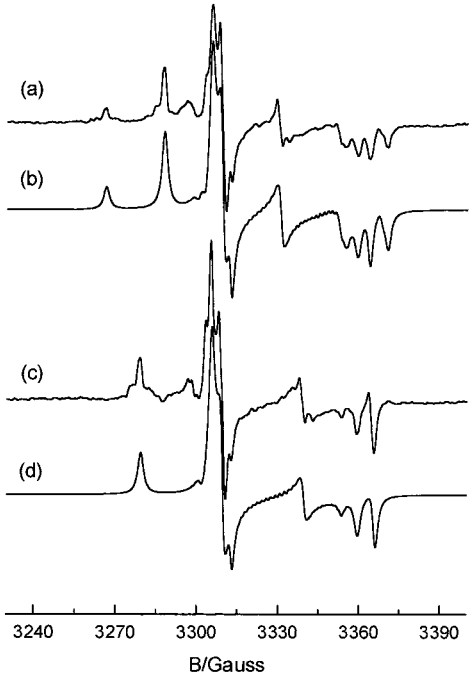

Figure 4. $^{14}N_2^-$ and $^{15}N_2^-$ on MgO. The EPR spectra have the same order as that in Figure 3.

(1.40) between the nuclear magnetic moments of the two isotopes. The agreement between experimental and simulated spectra in both cases is excellent and confirms the spin−Hamiltonian parameters listed in Table 1. The EPR spectra and corresponding simulations of the adsorbed $^{14}N_2$ and $^{15}N_2$ species on MgO are also shown in Figure 4 for completeness. Only minor differences were observed in the **g** and **A** values compared to those of CaO; the spin−Hamiltonian parameters are listed in Table 1.

The formation of N_2^- on both oxides was found to depend on the nitrogen surface coverage, since the EPR spectrum varied as a function of the N_2 equilibrium pressure. This effect is illustrated in Figure 5 for N_2 adsorption on the electron-rich CaO surface. A progressive appearance of the N_2^- signal can be observed at the expense of the F_S^+(D) signal as the pressure is raised. The N_2^- signal remains weak up to an equilibrium pressure of 40 Torr, after which the signal increases significantly and reaches a maximum intensity at a pressure (60 Torr), corresponding to a monolayer of physisorbed N_2 according to the BET theory.[39] No further increase in intensity is observed at higher pressures where multilayer physisorption occurs. If, on the other hand, the temperature of the system is increased to room temperature in the presence of the adsorbed N_2 layer, a series of spectra almost identical to Figure 5 is obtained, but with at inverted order, confirming that the surface N_2^- complex is destroyed upon desorption.

3.3. Nature of the Adsorption Site. Careful inspection of the N_2^- signal generated on MgO containing F_S^+(D) or F_S^+(H) centers reveals that each of the main lines in the N_2^- spectrum generated over the F_S^+(D) centers (Figure 6a) are split into doublets in the case of N_2^- formed over the F_S^+(H) centers (Figure 6b). This weak superhyperfine splitting of less than 1 G indicates that a single proton ($I = {}^1/_2$) interacts with the N_2^- radical, and this proton must originate from the original surface OH group associated with the F_S^+(H) center. This indicates that the adsorption site for N_2^- is the same assembly of ions constituting the electron trap for the surface electron. The hypothesis is further justified by considering the facile and reversible electron transfer from N_2^- back to the surface trap, and this seems possible only if the adsorbed molecule and electron trap are close to each other. The ^{1}H superhyperfine (shf) coupling constants (Figure 6b) are very small and will be further investigated using pulsed ENDOR. Nevertheless, a preliminary interpretation of the ^{1}H shf structure within the dipolar approximation indicates that the proton is equidistant from both nitrogen atoms forming an isosceles triangle.

3.4. Spin−Hamiltonian Parameters and Electron Spin Density on N_2^-. The adsorbed species identified on MgO and CaO can be classified in terms of a true N_2^- radical anion, and in the limits of a "chemical" approach, this represents the best description for the observed species. This anion has been previously observed only in the bulk of solid (matrixes including single crystals of various azides (K, Na, Ba)[40−42] or alkali-halides[43]) and formed by the photodecomposition of N_3^-. The reported **g** and **A** tensors were remarkably similar to those found

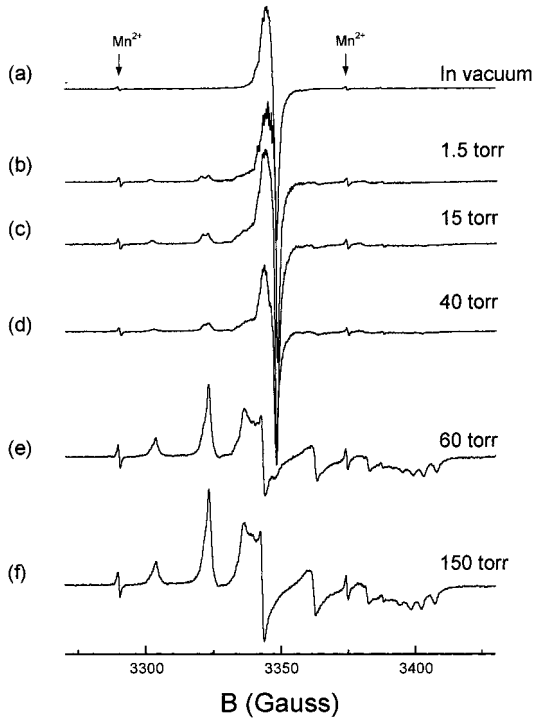

Figure 5. EPR spectra of CaO containing surface F_S^+(D) centers under increasing N_2 pressure. Spectra recorded at 77 K.

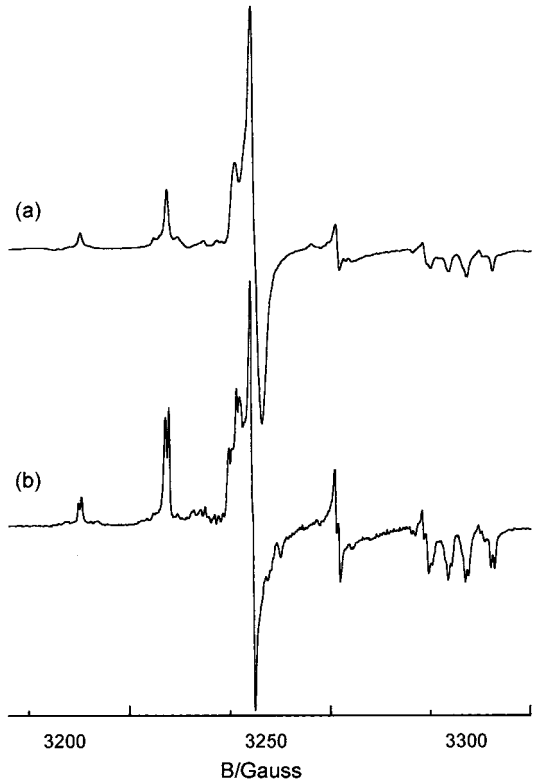

Figure 6. Comparison of the spectra of $^{14}N_2^-$ obtained on CVD MgO containing (a) F_S^+(D) and (b) F_S^+(H).

in this work (Table 1). Despite the polycrystalline nature of the solids used in this work, the powder EPR spectra exhibit better resolution than the above-mentioned N_2^- single-crystal spectra.

g Tensor. The **g** tensor of the adsorbed species in Figures 2−5 is in agreement with that expected for the $^2\Pi_{1/2}$ state of an 11-electron radical like N_2^-. The electronic configuration of such a species (isoelectronic with NO, CO^-, and O_2^+) is characterized by the presence of a single unpaired electron in the π antibonding orbitals. The EPR spectrum can only be observed for such a radical if the degeneracy of the two antibonding orbitals is lifted by an asymmetric electric field, such as that exerted by a surface cationic site. To a first approximation, the unpaired electron is confined to the π^* orbital with lower energy. Scheme 2a reports the axis system adopted in the following discussion and the relevant energy levels of the adsorbed N_2^- species. According to convention, the *z* direction is chosen along the internuclear axis.[44] The geometry of the system, with the radical ion parallel to the surface, is deduced from the magnetic equivalence of the two nitrogen atoms. The electronic configuration produces an orthorhombic **g** tensor whose elements can be obtained by adapting the equations of Zeller, Shuey, and Känzig,[45] (originally derived for $^2\Pi_{3/2}$ states) to the N_2^- case, in agreement with the treatment performed by Brailsford et al[43] for N_2^- in KCl single crystal. A slightly simplified form of these equations, which are suited to the $^2\Pi_{1/2}$ state, with the unpaired electron on the π^*_y orbital (vide infra) are given as

SCHEME 2

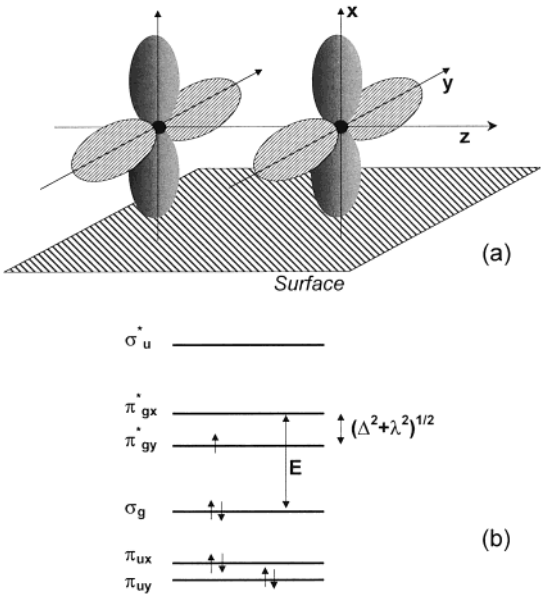

$$\mathbf{g}_{zz} = \mathbf{g}_e - 2\lambda \sin 2\alpha \quad (2)$$

$$\mathbf{g}_{yy} = \mathbf{g}_e \cos 2\alpha + (\lambda/E)(1 + \cos 2\alpha + \sin 2\alpha) \quad (3)$$

$$\mathbf{g}_{xx} = \mathbf{g}_e \cos 2\alpha + (\lambda/E)(\cos 2\alpha - \sin(2\alpha - 1)) \quad (4)$$

where λ is the spin−orbit coupling constant, *E* and Δ are the energy differences shown in Scheme 2b, and tan 2α is defined as λ/Δ. The degeneracy of the π^*_y and π^*_x orbitals is lifted by the spin−orbit interaction (λ) and the orthorhombic crystal-field at the surface measured by a splitting parameter (Δ). It follows from the above equations that $\mathbf{g}_{yy} > \mathbf{g}_{xx} > \mathbf{g}_{zz}$, and the only important shift from $\mathbf{g}_e$ is expected for one component ($\mathbf{g}_{zz}$), as indeed experimentally observed (Table 1). Due to the excellent resolution of the experimental spectra and the high accuracy of the **g** values derived by simulation, the molecular parameters λ, Δ, and *E* for N_2^- trapped on MgO and CaO can be calculated by fitting the corresponding experimental **g** tensors to the above equations (2−4). The results of the optimization are listed in Table 2, where the **g** values recalculated by introducing the best-fit molecular parameters back into eqs 2−4 are also reported for completeness. The advantage of this procedure is that by allowing λ to differ from the free atom value, we can account for partial delocalization of the unpaired electron onto the

TABLE 2: Molecular Parameters (Spin−Orbit Coupling Constant and Energy Splittings) Derived from the Experimental g Tensor Values[a]

	parameters/eV			experimental			calculated		
species	λ	Δ	E	g_{xx}	g_{yy}	g_{zz}	g_{xx}	g_{yy}	g_{zz}
N_2^-/MgO	0.0082	0.537	7.72	2.0018	2.0042	1.9719	2.002	2.0042	1.9719
N_2^-/CaO	0.0062	0.355	4.42	2.0006	2.0048	1.9677	2.0019	2.0048	1.9677

[a] The last three columns report the **g** values calculated on the basis of the optimized molecular parameters.

surface. If we assume alternatively that the unpaired electron is in the π^*_x orbital, a much less satisfactory fit was obtained, so this latter possibility was rejected.

Comparing the λ values found for N_2^- trapped at the surface of MgO and CaO (0.0082 and 0.0062 eV, respectively) with the corresponding atomic value ($\lambda^0 = 0.0092$ eV),[46] we found a considerable reduction factor l ($l = \lambda/\lambda^0$) in the two cases (0.9−0.7). These values are close to that found earlier for N_2^- in potassium azide[40] and indicate a non-negligible delocalization of the N_2^- electron into the surroundings. Furthermore, in the case of N_2^- on CaO, the lower values for the molecular parameters λ, Δ, and E, compared to the value of N_2^-/MgO, indicate an enhanced covalency of the bonding with the adjacent atoms. It is worth noting that a similar phenomenon was also observed in the case of O_2^- radicals stabilized on various alkali metal cations. A monotonic increase in the covalent character of the bonding between O_2^- and the Na^+, K^+, Rb^+, and Cs^+ centers could be readily deduced from the EPR spectra.[47]

^{14}N Hyperfine Tensor. The **A** tensor of the ^{14}N hyperfine may be written as

$$\mathbf{A} = a_{iso} I + \mathbf{T} \tag{5}$$

where a_{iso} is the isotropic component (Fermi contact) of the hyperfine interaction and **T** is the anisotropic interaction term. Analysis of the hyperfine tensor requires knowledge of the sign of the nitrogen coupling constants that cannot be derived from powder spectra. However, on the basis of theoretical calculations (vide infra), the only reasonable alternative is $\mathbf{A}_{yy} > 0$, while $\mathbf{A}_{xx}$ and $\mathbf{A}_{zz} < 0$, since all other combinations lead to unacceptable results. The choice of signs implies that $a_{iso} > 0$, and it is also consistent with that adopted for the hyperfine analysis of N_2^- trapped in various single crystals,[40−44] for which a_{iso} is expected to be positive.[44] The largest value of the hyperfine tensor corresponds to the y direction determined by π_y^*, i.e., the orbital constituting the SOMO. The **T** tensor derived from eq 5 is not axial but can be decomposed into two traceless components ($2a,-a,-a$) and ($-b,2b,-b$) as follows:

$$^{N}A(MgO) = \begin{vmatrix} -2.9 & & 0.87 & & -8.57 \\ & 21.5 & & -0.43 & & 17.13 \\ -4.2 & & -0.43 & & -8.57 \end{vmatrix} = 4.8 + \begin{vmatrix} -7.7 & & 0.87 & & -8.57 \\ & 21.5 & & -0.43 & & 17.13 \\ -4.2 & & -0.43 & & -3.8 \end{vmatrix}$$

$$^{N}A(CaO) = \begin{vmatrix} -2.5 & & 1.20 & & -8.10 \\ & 20 & & -0.60 & & 16.2 \\ -4.3 & & -0.60 & & -8.10 \end{vmatrix} = 4.4 + \begin{vmatrix} -6.9 & & 1.20 & & -8.10 \\ & 20 & & -0.60 & & 16.2 \\ -4.3 & & -0.60 & & -3.7 \end{vmatrix}$$

The decomposition along the x and y directions indicates a partial admixture of the π_x orbital to π_y, since the two orbitals are close in energy and are coupled via spin−orbit interactions. Using the reported atomic value [48] of the dipolar ^{14}N constant as $B^0 = 4/5\mathbf{g}_N\beta_n\langle r^{-3}\rangle_{2p} = 39.62$ G, we can assess the spin density on the nitrogen 2p orbitals by direct comparison of the experimental $2a$ and $2b$ values to the atomic anisotropic coupling constant of nitrogen using the classic formulas $\rho_{2py} = c_{2py}^2 = 2b/B^0$ and $\rho_{2px} = c_{2px}^2 = 2a/B^0$. The resultant spin densities for both oxides are listed in Table 3.

TABLE 3: Spin Densities in the Various Nitrogen Orbitals for N_2^- Ions on MgO and CaO Derived from Experimental Spectra[a]

species	$\rho(2p_x)$	$\rho(2p_y)$	c_{2s}^2	$\rho(2s)$	$\rho(N)_{total}$	ρ_{surf}
N_2^-/MgO	0.022	0.432	0.0052	0.0074	0.919	0.081
N_2^-/CaO	0.03	0.409	0.0046	0.0068	0.888	0.112

[a] The spin density on the solid is $\rho_{surf} = 1 - \rho(N)_{total}$.

The isotropic coupling arises from both a direct contribution of the nitrogen 2s orbital to the SOMO and the polarization of the ns orbitals by the unpaired electron localized on the orthogonal π^* orbitals. Following our previous analysis for a Cu^+−NO adduct,[49] we can combine the Hunter−Symons polarization formula[50] with the classic expression for $a_{iso} = A^0_{iso}c_{2s}^2$

$$a_{iso} = A^0_{iso}\, c^2_{2s} + \frac{A^0_{iso}}{100}(\rho_{N_a} U^N - \rho_{N_b} U^{N-N}) \tag{6}$$

ρ_{Na} and ρ_{Nb} are the spin densities on the 2p orbitals of both N atoms (calculated from the analysis of the dipolar part of the hyperfine tensor), $U^N = 2.5$ and $U^{N-N} = 2$ are the polarization constants for the N atom and for the adjacent atom, respectively, and $A^0_{iso} = 8\pi/3g_N\beta_n|\psi(0)|^2 = 646.2$ G is the atomic nitrogen isotropic hyperfine constant.[48] The contribution of the polarization term to the isotropic coupling was assessed as 1.47 and 1.42 G for MgO and CaO, respectively. The remaining part (3.33 and 2.98 for MgO and CaO, respectively) is thus assigned to the direct delocalization mechanism and was used to calculate the c^2_{2s} coefficient. The results indicate that the c_{2s}^2 values are very small, in agreement with the pronounced $^2\Pi$ nature of the N_2^- radical. The total spin density on the adsorbed radical is thus $\rho(N)_{total} = 2[\rho(2p_x) + \rho(2p_y) + c^2_{2s})]$, while on the surface, $\rho_{surf} = 1 - \rho(N)_{total}$. The corresponding values are listed in Table 3. The total spin density on the N atoms is close to unity, justifying the description of the observed phenomenon in terms of a true reversible electron transfer from the F_S^+ center toward the adsorbed nitrogen

$$F_S^+(H) + N_2 \leftrightarrows F_S^{2+}(H)/N_2^-$$

Considering the negative electron affinity of dinitrogen, the principal driving force for this process is provided by the strong electrostatic interaction of the N_2^- anion with the surface Madelung potential.

3.5. Ab initio Calculations: Charge-Transfer Mechanism. The charge-transfer character of N_2 interacting with the surface F_S^+ center was recently performed using HF calculations,[19] and a more refined description at the DFT-B3LYP level, where correlation effects are taken into account, is now presented. Full geometry optimizations and sections of the potential energy surface have been performed. In the latter case, the N−N distance was fixed at an intermediate value between N_2 and N_2^-, while the surface−N_2 distance was optimized (Figure 7). The N_2 molecule has been adsorbed with the molecular axis parallel to the surface and aligned toward the O anions (Figure

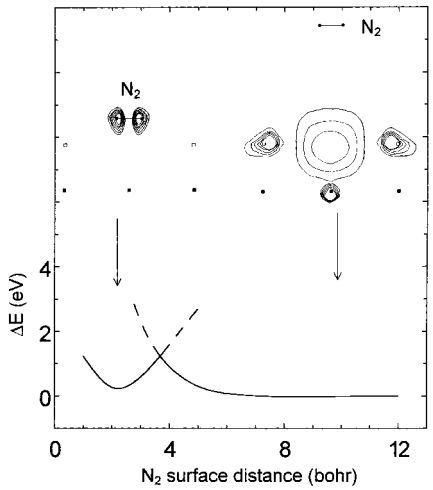

Figure 7. Potential energy curves for the interaction of N_2 with an F_S^+ center (repulsive curve) and of N_2^- with an F_S^{2+} center (attractive curve), computed at the DFT level. The isocontour lines of the spin density calculated at the DFT level show the different localization of the unpaired electron for large and short N_2−MgO distances. The plots are drawn in a plane normal to the MgO surface containing the N_2 molecule ($y = 0$), with intervals of 0.002 e/au^3. Empty squares, O atoms; filled squares, Mg atoms; black circles, N atoms.

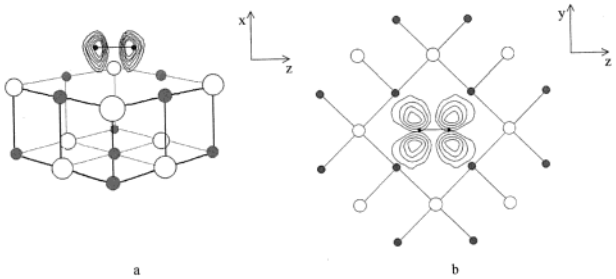

Figure 8. Spin density plots of the unpaired electron localized in the π^* component of the N_2 molecule (configuration $[a_2(yz)]^1$). (a) Side view and (b) top view (the spin density is plotted in the plane parallel to the surface which contains the N_2 molecule). Lines are drawn in intervals of 0.002 e/au^3. White spheres, O; gray spheres, Mg; black spheres, N.

8). Two possible states are found, a "neutral one", F_S^+/N_2, with the unpaired electron trapped in the vacancy site, and a "charge transfer" state, F_S^{2+}/N_2^-, where the unpaired electron is transferred to the adsorbed molecule. The different nature of the two states is clearly shown by the spin density plots at large and short surface−N_2 distances. In particular, in the minimum of the F_S^{2+}/N_2^- state, the spin density plot (Figure 8) clearly shows that the spin is localized on a N_2 π orbital, consistent, with the occurrence of a nearly complete charge transfer. The neutral curve is repulsive, while the charge-transfer one presents a pronounced minimum at short surface−N_2 distances, Figure 7. Here the surface complex is stabilized by a strong F_S^{2+}−N_2^- electrostatic interaction. The HF results showed that the F_S^{2+}/N_2^- complex is slightly higher in energy than the $F_S^+ + N_2$ dissociation limit,[19] suggesting the existence of a metastable N_2^- species similar to the metastable CO^- observed in similar conditions.[51] Several factors can contribute to this result: the absence of correlation effects, the neglect of surface relaxation, and basis set limitations. In this work, we have carefully considered these points by performing DFT calculations with large basis sets and full geometry optimization.

The optimal geometrical parameters of the F_S^{2+}/N_2^- surface complex obtained at the B3LYP level are shown in Table 4. Two possible orientations for the N_2 molecule have been considered, parallel and normal to the surface. The two orientations are similar in energy (the difference is only 0.17 eV), but the normal form is slightly preferred. After the inclusion of BSSE correction, both are metastable with respect to dissociation into "neutral" fragments. This small metastability, −0.27 eV for the parallel orientation and −0.10 eV for the normal one, could be easily due to computational details, for instance, the exchange-correlation functional used. It can only be concluded that the formation of N_2^- at a five-coordinated F_S^+ center is almost thermoneutral. These results are similar to HF ones,[19] indirectly confirming the electrostatic nature of the interaction and the noncritical correlation effects. In the minimum structure, the Mg^{2+} and O^{2-} ions around the vacancy change positions slightly with respect to the case without adsorbed N_2. Both Mg^{2+} and O^{2-} nearest neighbors move outward by about 1−2% with respect to the center of the vacancy; the displacement of the next nearest O^{2-} ions is negligible (0.5%). The small relaxation of the cavity is due to the fact that the electron is transferred to the adsorbed molecule but not completely removed from the vacancy as would be the case of F_S^+ ionization with formation of an F_S^{2+} center. In this case, the ion displacements are on the order of 5%. The computed N−N distance in the surface N_2^- complex is elongated by about 8% compared to the gas-phase, indicating a partial activation of the N−N bond consistent with the occupation of the π^* antibonding orbital of N_2 by the unpaired electron.

TABLE 4: Optimal Geometrical Parameters and Adsorption Energies for N_2 Adsorbed on a F_S^+ Center of MgO from Full Geometry Optimization

	parallel	normal[a]
$x(N_2)$, Å	1.192	0.635, 1.829
r(N−N), Å[b]	1.175	1.194
spin density at N	0.44	0.29, 0.63
D_e ($F_S^{2+}/N_2^- \rightarrow F_S^+ + N_2$),[c] eV	0.19	0.32
D_e ($F_S^{2+}/N_2^- \rightarrow F_S^+ + N_2$) with BSSE,[c] eV	−0.27	−0.10

[a] First number for $z(N_2)$ and spin density at N refers to the N atom nearest to the surface. [b] r(N−N) free = 1.096 Å. [c] D_e is the dissociation energy for the process indicated in the table and is defined to be positive for bound systems.

The higher stability of the normal orientation of N_2 is not in line with the experimental observation of equivalent N nuclei. In fact, the spin density for normal adsorption is asymmetrically distributed over the two N atoms. However, given the very small energy difference between the two orientations and the assumptions about the structure of the F center, we do not consider this as a major deviation from experimental findings. It should also be mentioned that two parallel orientations of the N_2 molecule are possible, one with the molecular axis directed toward the O anions (Figure 8) and one rotated by 45°. According to our calculations, however, the energy difference between the two configurations is very small (less than 0.1 eV) and could result in a fluxional behavior at temperatures above liquid nitrogen.

The analysis of the potential energy curves at the DFT level (Figure 7) confirms that the formation of the charge-transfer complex implies a crossing between an unbound state (F_S^+/N_2) and a bound one (F_S^{2+}/N_2^-) and suggests that only a small barrier (not investigated in detail) separates the F_S^{2+}/N_2^- minimum from the $F_S^+ + N_2$ dissociation limit. This is consistent with the observed facile desorption of nitrogen in its neutral molecular form.

The spin distribution and hyperfine interactions of the F_S^{2+}/N_2^- surface complex were considered for the parallel orientation.

TABLE 5: Calculated Hyperfine Coupling Constants for Gas-Phase N_2^- and for the Same Ion Adsorbed on an F_S^{2+} Center on MgO

	^{14}N/G						
model	A_1	A_2	A_3	$\mathbf{a_{iso}}$	B_1	B_2	B_3
gas-phase N_2^-	17.7	−5.4	−5.9	**2.1**	15.6	−7.5	−8.0
F_S^{2+}/N_2^-	18.1	−6.7	−7.1	**1.4**	16.7	−8.1	−8.5
F_S^{2+}/N_2^- on MgO	21.5	−2.9	−4.2	**4.8**	16.7	−7.7	−9.0
experimental values							

The computed value of 88% spin density on N_2 is in excellent agreement with the EPR data (92%) (Table 3). The N 2s contribution to the unpaired electron wave function is negligible, while the N 2p contribution is close to 100%. This computational result is also fully consistent with the EPR analysis. The isotropic and anisotropic parts of the **A** tensor, computed at the spin polarized DFT-B3LYP level, are shown in Table 5. For comparison, the values of gas-phase N_2^- are also given; these have been computed for the same distance that N_2^- has in the surface complex. One can notice two things: an excellent agreement of the anisotropic part of the tensor **T** with that derived from EPR spectrum and the slight underestimate of the isotropic a_{iso} values. In general, however, the remarkable agreement found between computed and observed values as well as for free N_2^- and the F_S^{2+}/N_2^- complex provides strong support for the assignment of a surface formed N_2^- species.

Analysis of the **g** tensor allows one to deduce the splitting of the π^* energy levels of N_2 due to the surface electric field. This quantity formally corresponds to the energy required to excite one electron from the singly occupied π^*_y level (parallel to the surface) to the π^*_x one (normal to the surface) and can be obtained from quantum-chemical calculations as the energy difference of the two states, $[a_2(yz)]^1$ and $[b_1(xz)]^1$. In this work, an approximate approach was adopted by considering the energy of the two electronic configurations of adsorbed N_2^- $[a_2(yz)]^1$ and $[b_1(xz)]^1$, respectively, from HF calculations (convergence for the two states at the DFT level was not possible). We found that for the N_2 orientation shown in Figure 8, the $[a_2(yz)]^1$ configuration (π^* component parallel to the surface) is lower in energy than the $[b_1(xz)]^1$ one by 0.45 eV. Considering the neglect of correlation effects and the other limitations of the model, these results are also in excellent agreement with the EPR parameters.

3.6. Concluding Remarks. An unusual reversible electron-transfer process from surface trapped electrons on MgO and CaO to adsorbed N_2 molecules has been evidenced in this paper. Both EPR and quantum chemical calculations have confirmed that approximately 90% of the electron spin is confined to the π_y^* antibonding orbitals of the resulting N_2^-. This species can therefore be classified in chemical terms as a true N_2^- radical anion, which has only been previously observed in irradiated azides[40−43] or as short-lived temporary ions.[34] The N_2^- anion was found to be adsorbed parallel to the surface anion vacancy ("side-on" structure; Figure 8), and the ionicity of the bonding with the surface was higher on MgO than CaO. Increasing the temperature causes the N_2 molecule to desorb from the surface and the unpaired electron to become trapped again in the original vacancy. Excellent agreement was found between the EPR results and the theoretical data, both for the observed electron-transfer step between adsorbed N_2 and the surface F_S^+ centers and for the molecular and magnetic parameters of the resultant N_2^- species.

The EPR spectra and associated spin Hamiltonian parameters of the N_2^- anion were particularly well resolved and unambiguous due to the good crystallinity of the solid and also due to the absence of any heterogeneous distribution of radicals which could produce slightly different spin−Hamiltonian parameters, as observed for O_2^- on the same system.[16,52] This is an important observation, indicating that the electron-transfer process is selective and does not involve all of the heterogeneous surface F_S^+ centers (see section 3.2). The reason of this specificity originates from the high positive value of the $[IP(F_S^+) - EA(N_2)]$ term, the difference between the (high) ionization potential of the surface F centers and the (negative) electron affinity of the N_2 molecule. Among the various families of the surface F centers,[13,14] there is probably only one family for which $[IP(F_S^+) - EA(N_2) + \Delta W] < 0$, where ΔW is the $N_2^- - F_S^{2+}$ interaction energy. This latter family of sites must have a high Madelung potential which compensates the unfavorable (IP-EA) term and thereby produces a thermodynamically favorable electron-transfer step. Such conditions could be satisfied by vacancies at the (100) faces, unlike the unfavorable conditions present at other sites (at edges and corners) with lower Madelung constants. This hypothesis will be explored by further theoretical work.

The present results may have important implications in the field of dinitrogen activation, where N_2^- formation is clearly a crucial step. Although the current surface N_2^- anion has a $-^1/_2$ oxidation state and an increased N−N bond of approximately 8%, the anion is only metastable and reversibly desorbs from the surface as molecular nitrogen as the temperature is raised. Nevertheless, the current results remain promising considering that these alkaline-earth oxides which support the N_2^- anion are also well-known to activate the H_2 molecule. Therefore, despite the limitations imposed by the reversibility of the N_2 reduction, we think that the ability to activate both N_2 and H_2 molecules should rejuvenate attention to the surface chemistry of alkaline-earth oxides.

Acknowledgment. The present work is part of a project coordinated by A. Zecchina and cofinanced by the Italian Murst (Cofin98 Area 03) and has also been supported by INFM (Istituto Nazionale Fisica della Materia) through a PAIS project. M.C. thanks the EC for a Marie Curie Research Fellowship (ERBFMBICT98 3508).

References and Notes

(1) Jennings, J. R. *Catalytic Ammonia Synthesis*; Plenum: New York, 1991.
(2) Leigh, G. J. *Science* **1998**, *279*, 506.
(3) Henderson, R. A.; Leigh, G. J.; Pickett, C. J. *Adv. Inorg. Chem. Radiochem.* **1983**, *27*, 197.
(4) Pelikan, P.; Boca, R. *Coord. Chem. Rev.* **1984**, *55*, 55.
(5) Orme-Johnson, W. H. *Science* **1992**, *257*, 1639.
(6) Kim, J.; Rees, D. C. *Biochemistry* **1994**, *33*, 389.
(7) Deng, H.; Hoffmann, R. *Angew. Chem., Int. Ed. Engl.* **1993**, *32*, 1062.
(8) Bazhenova, T. A.; Shilov, A. E. *Coord. Chem. Rev.* **1995**, *144*, 64.
(9) Giamello, E.; Murphy, D.; Ravera, L.; Coluccia, S.; Zecchina, A. *J. Chem. Soc., Faraday Trans.* **1994**, *90*, 3167.
(10) Murphy, D.; Giamello, E. *J. Phys. Chem.* **1995**, *99*, 15172.
(11) Giamello, E.; Paganini, M. C.; Murphy, D.; Ferrari, A. M.; Pacchioni, G. *J. Phys. Chem. B* **1997**, *101*, 971.
(12) Chiesa, M.; Paganini, M. C.; Giamello, E.; Murphy, D. M. *Langmuir* **1997**, *13*, 5306.
(13) Paganini, M. C.; Chiesa, M.; Giamello, E.; Martra, G. M.; Coluccia, S.; Murphy, D. M. *Surf. Sci.* **1999**, *421*, 240.
(14) Murphy, D.; Farley, R. D.; Purnell, I. J.; Rowlands, C. C.; Yacob, A. R., Paganini, M. C.; Giamello, E. *J. Phys. Chem. B* **1999**, *103*, 1944.
(15) D'Ercole, A.; Giamello, E.; Pisani, C.; Ojamäe, L. *J. Phys. Chem. B* **1999**, *103*, 3872.
(16) Pacchioni, G.; Ferrari, A. M.; Giamello, E. *Chem. Phys. Lett.* **1996**, *255*, 58.
(17) Anpo, M.; Che, M.; Fubini, B.; Garrone, E.; Giamello, E.; Paganini, M. C. *Topics Catal.* **1999**, *8*, 189.

(18) Giamello, E.; Murphy, D.; Marchese, L.; Martra, G. M.; Zecchina, A. *J. Chem. Soc., Faraday Trans.* **1993**, *89*, 3715.
(19) Giamello, E.; Paganini, M. C.; Chiesa, M.; Murphy, D. M.; Soave, R.; Pacchioni, G.; Rockenbauer, A. *J. Phys. Chem. B* **2000**, *104*, 1887.
(20) Diwald, O.; Hofmann, P.; Knözinger, E. *Phys. Chem. Chem. Phys.* **1998**, *1*, 713.
(21) Pacchioni, G., Bagus, P. S., Parmigiani, F., Eds. *Cluster Models for Surface and Bulk Phenomena*; NATO ASI Series B; Plenum: New York, 1992; Vol. 283.
(22) Sauer, J.; Ugliengo, P.; Garrone, E.; Saunders, V. R. *Chem. Rev.* **1994**, *94*, 2095.
(23) Colbourn, E. A. *Surf. Sci. Rep.* **1992**, *15*, 281.
(24) Pacchioni, G.; Ferrari, A. M.; Marquez, A. M.; Illas, F. *J. Comput. Chem.* **1997**, *18*, 617.
(25) Ferrari, A. M.; Pacchioni, G. *Int. J. Quantum Chem.* **1996**, *58*, 241.
(26) Winter, N. W.; Pitzer, R. M. *J. Chem. Phys.* **1988**, *89*, 446.
(27) Nygren, M. A.; Pettersson, L. G. M.; Barandiaran, Z.; Seijo, L. *J. Chem. Phys.* **1994**, *100*, 2010.
(28) Mejias, J. A.; Marquez, A. M.; Fernandez Sanz, J.; Fernandez-Garcia, M.; Ricart, J. M.; Sousa, C.; Illas, F. *Surf. Sci.* **1995**, *327*, 59.
(29) Stevens, W. J.; Basch, H.; Krauss, M. *J. Chem. Phys.* **1984**, *81*, 6026.
(30) Barandiaran, Z.; Seijo, L. *J. Chem. Phys.* **1988**, *89*, 5739.
(31) Pisani, C. *J. Mol. Catal.* **1993**, *82*, 229.
(32) Becke, A. D. *Phys. Rev. A* **1988**, *38*, 3098.
(33) Lee, C.; Yang, W.; Parr, R. G. *Phys. Rev. B* **1988**, *37*, 785.
(34) Gutsev, G. L., Rozyczko, P. B.; Bartlett, R. J. *J. Chem. Phys*. **1999**, *110*, 5137.
(35) Ditchfield, R.; Hehre, W. J.; Pople, J. A. *J. Chem. Phys.* **1971**, *54*, 724.
(36) Boys, S.; Bernardi, F. *Mol. Phys.* **1970**, *19*, 553.
(37) Dupuis, M.; Johnston, F.; Marquez, A. *HONDO 8.5*, per CHEM-Station; IBM Co.: Kingston, U.K., 1994.
(38) Frisch, M. J.; Trucks, G. W.; Schlegel, H. B.; Scuseria, G. E.; Robb, M. A.; Cheesman, J. R.; Zakrzewski, V. G.; Montgomery, J. A.; Stratmann, R. E.; Burant, J. C.; Dapprich, S.; Millam, J. M.; Daniels, A. D.; Kudin, K. N.; Strain, M. C.; Farkas, O.; Tomasi, J.; Barone, V.; Cossi, M.; Cammi, R.; Mennucci, B.; Pomelli, C.; Adamo, C.; Clifford, S.; Ochterski, J.; Petersson, G. A.; Ayala, P. Y.; Cui, Q.; Morokuma, K.; Malick, D. K.; Rabuck, A. D.; Raghavachari, K.; Foresman, J. B.; Cioslowski, J.; Ortiz, J. V.; Stefanov, B. B.; Liu, G.; Liashenko, A.; Piskorz, P.; Komaromi, I.; Gomperts, R. L.; Martin, D. J.; Fox, T.; Keith, M. A.; Al-Laham, C. Y.; Peng, A.; Nanayakkara, C.; Gonzalez, R.; Challacombe, M.; Gill, P. M. W.; Johnson, B. G.; Chem, W.; Wong, M. W.; Andres, J. L.; Head-Gordon, M.; Repogle, E. S.; Pople, J. A. *Gaussian 98*; Gaussian Inc.: Pittsburgh, PA, 1998.
(39) Young, D. M.; Crowell, A. D. *Physical Adsorption of Gases*; Butterworth: London, 1962.
(40) Horst, R. B.; Anderson, J. H.; D. Milligan, E. *J. Phys. Chem. Solids* **1962**, *26*, 157.
(41) Gelerinter, E.; Silsbee, R. H. *J. Chem. Phys.* **1966**, *45*, 1703.
(42) Marinkas, P. L.; Bartram, R. H. *J. Chem. Phys.* **1968**, *48*, 927.
(43) Brailsford, J. R.; Morton, J. R.; Vannotti, L. E. *J. Phys. Chem.* **1969**, *50*, 1051.
(44) Atkins, P. W.; Symons, M. R. C. *The Structure of Inorganic Radicals*; Elsevier: Amsterdam, 1967.
(45) Zeller, M. R.; Shuey, R. T.; Kanzig, W. *J. Phys. Radium* **1967**, *28*, 81.
(46) Sunandana, C. S. *Bull. Mater. Sci*. **1998**, *21*, 1.
(47) Lindsay, D. M.; Herschbach, D. R.; Kwiram, A. L. *Chem. Phys. Lett*. **1974**, *25*, 175.
(48) Weil, J. A.; Bolton, J. R.; Wertz, J. E. *Electron Paramagnetic Resonance, Elementary Theory and Pratical Applications*; Wiley-Interscience: New York, 1994.
(49) Sojka, Z.; Che, M.; Giamello, E. *J. Phys. Chem. B* **1997**, *101*, 4831.
(50) Hunter, T. F.; Symons, M. R. C. *J. Chem. Soc. A* **1967**, 1770.
(51) Ferrari, A. M.; Pacchioni, G. *J. Chem. Phys.* **1997**, *107*, 2066.
(52) Giamello, E.; Murphy, D.; Garrone, E.; Zecchina, A. *Spectrochim. Acta* **1993**, *49A* (9), 1323.